Ab initio treatment of time-resolved x-ray scattering: Application to the photoisomerization of stilbene

Andrea Debnarova and Simone Techert[a)]
Max Planck Institute for Biophysical Chemistry, 37077 Göttingen, Germany

Stefan Schmatz[b)]
Institut für Physikalische Chemie, Universität Göttingen, 37077 Göttingen, Germany

(Received 30 June 2006; accepted 27 October 2006; published online 8 December 2006)

In this work we present a general theoretical outline for calculating time-dependent x-ray scattering signal changes from first principles. We derive a formalism for the description of atom-atom correlation functions as Fourier transforms of quantum-chemically calculated electron densities and show their proportionality to the molecular form factor. The formalism derived in this work is applied to the photoisomerization of stilbene. We can demonstrate that wide-angle x-ray scattering offers a possibility to study the changes in electron densities in nonperiodic complex systems, which renders it a suitable technique for the investigation of (bio)organic systems. © *2006 American Institute of Physics*. [DOI: 10.1063/1.2400231]

I. INTRODUCTION

In recent years, as the experimental challenges have been overcome, in biology and chemistry time-resolved x-ray diffraction and x-ray scattering have gained importance in the field of structural change characterization and dynamics of photoactivated molecular systems. The technical achievements at today's synchrotron sources (synchronization of ultrafast lasers to synchrotrons, enhancement of the x-ray flux, and high repetition frequency of the experiment) opened the possibility to investigate structural changes of weakly scattering matter like liquids and to study their structural responses upon photoexcitation up to a time resolution of 50 ps.[1–8] Technical breakthroughs in the development of plasma sources for the generation of x-rays make it possible to study ultrafast structural dynamics of condensed matter with and without periodical order.[9–12] As the technical improvements move forward,[13] and planned x-ray sources like the x-ray free electron laser (XFEL) or high-repetition rate sources like the energy recovery linac (ERL) come to a stage of building up,[14–16] new scientific questions have to be raised and answered, also from a theoretical point of view.

One of the questions which automatically arise and which has to be answered is to what extent a quantum-chemical treatment is required in order to describe the dynamics of ultrafast processes from an x-ray scattering point of view. In ultrafast spectroscopy, the concept of wave-packet dynamics has been successfully applied to the description of photoinduced ultrafast processes in molecular systems. Nonadiabatic transitions between the potential surfaces[17] as well as vibrational and/or rotational energy redistribution and relaxation processes can be expressed in a wave-packet propagation scheme leading to a description of ultrafast coherent molecular motions, dephasing, and energy dissipation into rovibrational eigenstates of the system. Even the control of wave-packet motion by focusing the delocalized wave packet has been proposed[18] and experimentally proved.[19] In time-resolved x-ray scattering experiments one observes the changes of scattered x-ray intensities as a function of time. Since the scattered x-ray intensities can be described as Fourier transformations (FTs) of electron densities, the time evolution of x-ray intensities can also be described in an electron density time-propagation scheme. In this work we introduce a description of electron density changes which is based on a full quantum-chemical approach from first principles.

The knowledge of the electron density of a particular electronic system is sufficient for the determination of the ground state energy of this system[20] as well as some of its important properties. Experimental techniques measuring this quantity are the x-ray scattering methods. Quantum-mechanical treatment (e.g., by Feil[21]) shows that in the first Born approximation scattering of a radiation field at a molecule with electron density $\rho(\mathbf{r})$ (where $\mathbf{r}$ is the position in 3D Euclidean space) leads to the well-known dependence of the scattering intensity I on the electron density which, normalized against the scattering intensity of one electron, reads

$$I = \left| \int d^3\mathbf{r}\rho(\mathbf{r})\exp(-i\mathbf{kr}) \right|^2. \quad (1)$$

Here $\mathbf{k}=(k_x,k_y,k_z)$ is the scattering vector.

Obtaining the electron density distribution of an electronic system from quantum-chemical methods is theoretically straightforward and as such the electron density has been suggested as a candidate for comparison of theoretical predictions and experiments[22,23] especially while studying the ground state structure of the system under consideration. The electron density is experimentally obtained most commonly from x-ray diffraction methods. The methods practically used for the electron density analysis are based on comparison between calculated and experimentally determined

[a)]Electronic mail: stecher@gwdg.de
[b)]Electronic mail: sschmat@gwdg.de

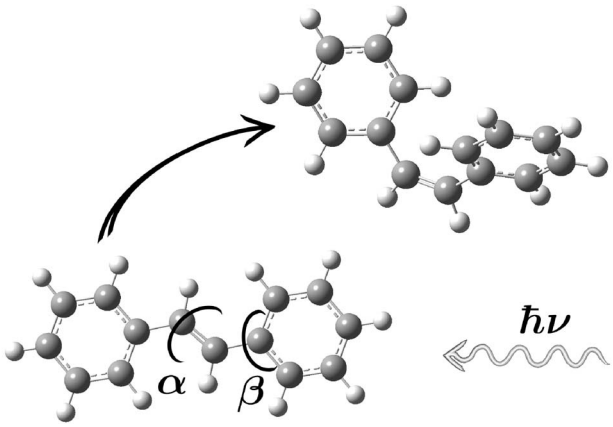

FIG. 1. Sketch of the photoisomerization geometries. The main photoisomerization angles are the dihedral α which corresponds to the large amplitude motion and the phenyl ring twisting angle β.

electron densities. By applying Laplacian analysis to the electron density distributions, and partitioning, chemical bonding and their changes could be characterized.[23] The relation between x-ray charge densities and chemical bonding has been summarized by Coppens.[24]

In this article, we take a closer look at the description of x-ray scattering as it is theoretically derived from the electron density distribution. The well-known relation between the electron density and the x-ray scattering signal can be used to directly calculate the scattering patterns. In the case of the electron density description in terms of Gaussian-type orbitals[25] (GTOs), the calculation is analytically exact. Moreover, we will show how this approach can be easily used for studying time-dependent processes in electronic systems.

As a model process for our time-dependent study we chose the photoisomerization of stilbene (Fig. 1) as a typical case of a photoinduced process. Generally, photoinduced processes are of utmost importance in biochemistry, practically they are being assessed in the growing field of organic electronics. Understanding these processes is essential for their successful application in the various branches of material science. Usually molecules containing a large number of atoms are involved and the potential energy surfaces are accordingly complex.

Due to its prototypical photochemical character, there has been done a large amount of experimental work on the photoisomerization of stilbene.[26–33] The transition from the excited state is almost 100% nonradiative and the process is irreversible. From a theoretical point of view, it is a system of moderate size, and the number of atoms involved can be easily assessed by most of the conventional quantum-chemical methods. Indeed stilbene has been already extensively studied theoretically.[34–36] The reason for the choice of this system for x-ray scattering measurements is also quite obvious. The large amplitude motion from planar 180° *trans* conformation to the 7° *cis* conformation, where the angles refer to the central dihedral angle, means strong electron density changes.[6] The signal from these changes is the most pronounced part of the scattering patterns. In this work, it will be demonstrated that on top of these changes fine structure of signal changes stemming from small variations of the electron density due to bonding and delocalization might be investigated.

A method of particular importance for studies of liquid samples, organic solutions, or biological samples is wide-angle x-ray scattering (WAXS).[37] The signal obtained in WAXS basically corresponds to the spherically averaged FT of the electron density of the studied system and naturally a large part of the information about the electron density is lost after this averaging. If we attempted to use this method for time-resolved studies, the experimental resolution would have to be very high in order to resolve all the information needed to describe the electron density changes in the system under investigation. The requirements on the experimental resolution depend on how detailed electron density changes we are interested to measure.

Since a liquid sample consists of the system (molecule) of interest, dissolved in a suitable solvent, we should shortly mention the effects of the solvent. The solvent should be chosen so that the signal from its structure is pronounced in the scattering pattern as little as possible and in a nondisturbing way. In the case of time-resolved measurements the strongest signal from the solvent corresponds to solvent heating.

Our goal is to estimate the possible application of x-ray scattering methods to the measurement of time-dependent processes. In Sec. II we will recollect the theoretical aspects needed for assessing the problem. Section III shows our approach applied to the stilbene molecule. We calculate the WAXS patterns from the FTs of the electron densities as given by density functional theory (DFT) calculations and compare the results with the WAXS patterns obtained from the classical Debye equation.

II. THEORY AND METHODOLOGY

A. Fourier transform of the electron density in terms of Gaussian-type atomic orbitals

The Debye scattering equation[37] results from classical (kinematic) x-ray scattering theory. The scattered intensity from a nonperiodic system (amorphous, liquid, or gaseous) in electron units is

$$I = \sum_m \sum_n f_m f_n \frac{\sin(kr_{mn})}{kr_{mn}}, \tag{2}$$

where f_m and f_n denote the atomic scattering factors of the mth and nth atom in the molecule, r_{mn} is the distance between those two atoms, and $k=(4\pi \sin\theta)/\lambda$, with θ being one-half of the scattering angle. In standard classical x-ray diffraction theory the atoms are modeled by a spherical distribution of electron density which is practically connected to the atomic scattering factor. Equation (2) describes the intensity from an amorphous sample (e.g., liquid or gaseous) as coming from the molecules which take random orientation in space. In this equation a model density is constructed from simple Gaussian-type functions placed at the atomic positions, Fourier transformed and averaged over spheres, and so all information about bonds and delocalized charges is discarded.

As in this simple model, also *ab initio* quantum-

chemical calculations rely on Gaussian functions, but not to model directly the electron density but rather the molecular wave function. Atomic orbitals are best represented by Slater-type orbitals (STOs) which are similar to the exact analytical solution of the Schrödinger equation for hydrogenlike atoms. These functions include the cusps of the *s* orbitals at the positions of the atomic nuclei which are responsible for the sharp peaks of the electron density at the nuclei. For computational reasons, GTOs, introduced by Boys[25] and nowadays used in most common electronic structure programs, are much more suitable due to the considerably facilitated evaluation of four-center two-electron integrals.

As the true electron density has very sharp maxima at the positions of the nuclei, a numerical approach starting from discrete electron densities would be computationally extremely expensive. However, the analytical FT is straightforward and exact for densities constructed from Gaussian-type functions. This representation of densities is natural if the quantum-chemical model is based on GTO basis sets. For example, in Hartree-Fock theory and Kohn-Sham DFT the density can be written as

$$\rho(\mathbf{r}) = \sum_{i=1}^{n_{\mathrm{occ}}} b_i |\phi_i(\mathbf{r})|^2, \tag{3}$$

with occupation numbers $b_i = 1,2$ and the number of occupied orbitals n_{occ}. The orbitals are expanded as

$$\phi_i(\mathbf{r}) = \sum_{\nu=1}^{N} C_{\nu i}\chi_\nu(\mathbf{r}), \tag{4}$$

where the N real basis functions χ_ν centered at $\mathbf{r}_\nu = (x_\nu, y_\nu, z_\nu)$ are defined as

$$\chi_\nu(\mathbf{r}) = \mathcal{N}_\nu (x - x_\nu)^{l_\nu}(y - y_\nu)^{m_\nu}(z - z_\nu)^{n_\nu} \times \exp(-\alpha_\nu(\mathbf{r} - \mathbf{r}_\nu)^2), \tag{5}$$

with normalization constant $\mathcal{N}_\nu$. Here, $l,m,n,\ldots = 0,1,2,\ldots$ denote *s*-, *p*-, and *d*-type functions, etc. Since the product of two Gaussians is a Gaussian, we obtain for the electron density

$$\begin{aligned}
\rho(\mathbf{r}) &= \sum_{i=1}^{n_{\mathrm{occ}}}\sum_{\mu=1}^{N}\sum_{\nu=1}^{N} b_i C_{\mu i} C_{\nu i}\chi_\mu(\mathbf{r})\chi_\nu(\mathbf{r}) \\
&= \sum_{i=1}^{n_{\mathrm{occ}}}\sum_{\mu=1}^{N}\sum_{\nu=1}^{N} b_i C_{\mu i} C_{\nu i}\mathcal{N}_\mu\mathcal{N}_\nu \exp\left(\frac{\alpha_\mu\alpha_\nu}{\alpha_\mu + \alpha_\nu}(\mathbf{r}_\mu - \mathbf{r}_\nu)^2\right) \\
&\quad \times (x - x_\mu)^{l_\mu}(x - x_\nu)^{l_\nu}(y - y_\mu)^{m_\mu}(y - y_\nu)^{m_\nu} \\
&\quad \times (z - z_\mu)^{n_\mu}(z - z_\nu)^{n_\nu}\exp(-\alpha_{\mu\nu}(\mathbf{r} - \mathbf{r}_{\mu\nu})^2) \\
&= \sum_{i=1}^{n_{\mathrm{occ}}}\sum_{\mu=1}^{N}\sum_{\nu=1}^{N} b_i C_{\mu i} C_{\nu i} B_{\mu\nu} \prod_{\xi=x,y,z} \\
&\quad \times (\xi - \xi_\mu)^{p_{\xi,\mu}}(\xi - \xi_\nu)^{p_{\xi,\nu}}\exp(-\alpha_{\mu\nu}(\xi - \xi_{\mu\nu})^2),
\end{aligned} \tag{6}$$

with

$$\alpha_{\mu\nu} = \alpha_\mu + \alpha_\nu, \tag{7}$$

$$B_{\mu\nu} = \mathcal{N}_\mu\mathcal{N}_\nu \exp\left(\frac{\alpha_\mu\alpha_\nu}{\alpha_\mu + \alpha_\nu}(\mathbf{r}_\mu - \mathbf{r}_\nu)^2\right), \tag{8}$$

and

$$\mathbf{r}_{\mu\nu} = \frac{\alpha_\mu\mathbf{r}_\mu + \alpha_\nu\mathbf{r}_\nu}{\alpha_\mu + \alpha_\nu}. \tag{9}$$

The FT of the electron density is then given by

$$\begin{aligned}
\mathcal{F}_{\mathbf{k}}\{\rho(\mathbf{r})\} &= \sum_{i=1}^{n_{\mathrm{occ}}}\sum_{\mu=1}^{N}\sum_{\nu=1}^{N} b_i C_{\mu i} C_{\nu i} B_{\mu\nu} \prod_{\xi=x,y,z} \mathcal{F}_{k_\xi}\{(\xi \\
&\quad - \xi_\mu)^{p_{\xi,\mu}}(\xi - \xi_\nu)^{p_{\xi,\nu}}\exp(-\alpha_{\mu\nu}(\xi - \xi_{\mu\nu})^2)\} \\
&= \sum_{i=1}^{n_{\mathrm{occ}}}\sum_{\mu=1}^{N}\sum_{\nu=1}^{N} b_i C_{\mu i} C_{\nu i} B_{\mu\nu} \\
&\quad \times \prod_{\xi=x,y,z} \mathcal{F}_{k_\xi}\left\{\sum_{j=0}^{p_{\xi,\mu}+p_{\xi,\nu}} c_j \xi^{p_{\xi,\mu}+p_{\xi,\nu}-j}\right. \\
&\quad \left.\times\exp(-\alpha_{\mu\nu}(\xi - \xi_{\mu\nu})^2)\right\},
\end{aligned} \tag{10}$$

with $c_j = f(\xi_\mu, \xi_\nu)$ and $c_0 = 1$.

The FT of a Gaussian function is again a Gaussian function,

$$\mathcal{F}_{\mathbf{k}}\{\exp(-\alpha(\mathbf{r} - \mathbf{r}_0)^2)\} = \sqrt{\frac{\pi}{\alpha}}\exp\left(-\frac{\mathbf{k}^2}{4\alpha}\right)\exp(i\mathbf{k}\mathbf{r}_0). \tag{11}$$

From the differentiation theorem of the FT,

$$\mathcal{F}_k[f'(\xi)] = -ik\mathcal{F}_k[f(\xi)], \tag{12}$$

we can easily calculate the FT of higher angular momentum atomic orbitals. For the FTs of the functions $f_l(\xi) = \xi^l \times \exp(-\alpha\xi^2)$ we obtain

$$\mathcal{F}_k\{f_{l+1}(\xi)\} = \frac{ik}{2\alpha}\mathcal{F}_k\{f_l(\xi)\} - \frac{l}{2\alpha}\mathcal{F}_k\{f_{l-1}(\xi)\}. \tag{13}$$

In particular, we find for the terms in Eq. (10),

$$\mathcal{F}_k\{\xi e^{-\alpha(\xi - \xi_0)^2}\} = \left(\frac{ik}{2\alpha} + \xi_0\right)\mathcal{F}_k\{e^{-\alpha(\xi - \xi_0)^2}\}, \tag{14}$$

$$\mathcal{F}_k\{\xi^2 e^{-\alpha(\xi - \xi_0)^2}\} = \left[\left(\frac{ik}{2\alpha} + \xi_0\right)^2 + \frac{1}{2\alpha}\right]\mathcal{F}_k\{e^{-\alpha(\xi - \xi_0)^2}\}, \tag{15}$$

and

$$\begin{aligned}
\mathcal{F}_k\{\xi^3 e^{-\alpha(\xi - \xi_0)^2}\} &= \left(\frac{ik}{2\alpha} + \xi_0\right)\left[\left(\frac{ik}{2\alpha} + \xi_0\right)^2 + \frac{3}{2\alpha}\right] \\
&\quad \times \mathcal{F}_k\{e^{-\alpha(\xi - \xi_0)^2}\},
\end{aligned} \tag{16}$$

for *p*-, *d*-, and *f*-type Gaussian functions. These results can also be obtained from the equation

$$\mathcal{F}_k\{\xi^n f(\xi)\} = (-i)^n \frac{\mathrm{d}^{(n)}\mathcal{F}_k\{f(\xi)\}}{\mathrm{d}k^n}. \tag{17}$$

Generally, the FT of the polynomial expression of the density (6) has the form

$$\mathcal{F}_{\mathbf{k}}\{\rho(\mathbf{r})\} = \sum_j C_j k_x^{l_j} k_y^{m_j} k_z^{n_j} \exp(-D_j \mathbf{k}^2 - i\mathbf{k}\mathbf{r}_{\mu\nu}). \tag{18}$$

Since we are interested in the x-ray scattering signal, the power of the absolute value of the FT of the electron density has to be averaged over the spherical angles,

$$I(k) = \frac{1}{4\pi}\int_0^{2\pi} d\varphi_k \int_0^{\pi} d\vartheta_k \sin\vartheta_k |\mathcal{F}_{\mathbf{k}}\{\rho(\mathbf{r})\}|^2, \tag{19}$$

where the index k in φ_k and ϑ_k denotes the spherical coordinates in k space. This definite integral contains exponentials of trigonometric functions caused by the shifts $\mathbf{r}_{\mu\nu}$ in (18) and we integrate it numerically using quadrature in polar coordinates, on a grid that is fine enough to give converged results.

B. Time dependence of the electron density and its Fourier transform

The density is implicitly time dependent via the expansion coefficients of the molecular orbitals $\{C_{\mu i}\}$ and via the position of the nuclei $\{\mathbf{r}_\mu\}$. Following a straightforward strategy we can obtain the time-dependent atom-atom correlation functions. First we solve the electronic Schrödinger equation within the Born-Oppenheimer approximation and so obtain the potential energy surfaces. Then we solve the nuclear Schrödinger equation and obtain a nuclear wave packet $\chi(\mathbf{R},t)$ as a function of time; here, $\mathbf{R}$ collectively denotes all nuclear coordinates. Then we calculate the expectation values of the nuclear coordinates by averaging over the nuclear wave packet and obtain in turn via the corresponding electronic wave functions the electron densities and therefrom their Fourier transformations as a function of time,

$$\begin{aligned}\rho(\mathbf{r}(t)) = &\sum_{i=1}^{n_{\mathrm{occ}}}\sum_{\mu=1}^{N}\sum_{\nu=1}^{N} b_i C_{\mu i}(t) C_{\nu i}(t) B_{\mu\nu}(t) \\ &\times \prod_{\xi=x,y,z} (\xi - \xi_\mu(t))^{p_{\xi,\mu}} (\xi - \xi_\nu(t))^{p_{\xi,\nu}} \\ &\times \exp(-\alpha_{\mu\nu}(\xi - \xi_{\mu\nu}(t))^2),\end{aligned} \tag{20}$$

with $p_\xi = l,m,n$ and

$$\begin{aligned}\mathcal{F}_{\mathbf{k}}\{\rho(\mathbf{r}(t))\} = &\sum_{i=1}^{n_{\mathrm{occ}}}\sum_{\mu=1}^{N}\sum_{\nu=1}^{N} b_i C_{\mu i}(t) C_{\nu i}(t) B_{\mu\nu}(t) \\ &\times \prod_{\xi=x,y,z} \mathcal{F}_{k_\xi}\left\{\sum_{j=0}^{p_{\xi,\mu}+p_{\xi,\nu}} c_j(t)\xi^{p_{\xi,\mu}+p_{\xi,\nu}-j} \right. \\ &\left. \times \exp(-\alpha_{\mu\nu}(\xi - \xi_{\mu\nu}(t))^2)\right\},\end{aligned} \tag{21}$$

with $c_j(t) = f(\xi_\mu(t), \xi_\nu(t))$ and $c_0 = 1$.

The more exact, but computationally extremely demanding method that can only be applied to small molecular systems, is to calculate the electron density at time t by averaging Eq. (20), parametrically dependent on $\mathbf{R}$, directly over the nuclear wave functions [see Eq. (22) in Sec. III C].

III. APPLICATION TO STILBENE

The photoisomerization of stilbene (Fig. 1) is a nonradiative process due to the conical intersection between the ground state and the S_1 state potential energy surfaces (PESs). After absorption of a UV photon *trans*-stilbene is excited from the electronic ground state (^1A_g) to the first excited singlet state (^1B_u). There is only a small barrier in the S_1 state between the Franck-Condon state and the conical intersection. After crossing this barrier, the process continues over the conical intersection ending up in the *cis* or *trans* conformation of the electronic ground state. In the following we will report on the calculations of the PES. This will be later required for the simulations of the single-molecule scattering (first), the averaged WAXS signal (second), and finally studies on the time evolution involving simple classical and wave-packet dynamics on a simplified PES.

A. Potential energy surface

The calculations of the ground and excited state PESs of stilbene were performed using the GAUSSIAN03 program package.[38] The results are graphically displayed in Fig. 2. We employed DFT for the electronic ground state calculations, or time-dependent DFT (TDDFT) for calculations of vertical excitation energies, using the B3LYP (Refs. 39 and 40) and B3P86 (Refs. 41 and 42) functionals as implemented in the Gaussian package. The choice of B3P86 can be supported by the fact that it was found to perform the best in calculating the excitation energies of ethene.[43] We use the 6-311++G(d,p) basis set in the calculation of the PES and the 6-31G(d) basis set in the calculation of the x-ray scattering.

The main geometry changes during the isomerization of the stilbene molecule (see Fig. 1) correspond to the dihedral angle α and the torsional angles β of the phenyl rings. The hydrogens at the central carbon atoms are also involved in the process. To avoid complications with the optimization of the geometries in the excited state we choose a simplified reaction path with an equidistant grid in the angles α, β and the angles of the central hydrogens from the optimized *trans* to the optimized *cis* geometry. The elongation of the central double bond as reported by Dietl *et al.*[34] and Improta and Santoro[35] is also taken into account. We employ this simplification in order to obtain an approximate PES, bearing in mind that the detailed energetics of the process is not the aim of our studies. The small barrier (measured[44] to be 1200 cm^{-1} and recently theoretically estimated[45] to 750 cm^{-1}) in the excited state between the Franck-Condon state and the 90° configuration where the nonradiative transition over the conical intersection occurs[45] is well reproduced (1197 cm^{-1} without correction for the zero-point energy) even on the simplified reaction path chosen for our calculations.

The conical intersection is the cause for difficulties in calculating the excited state reaction path. The TDDFT calculation has intrinsic limitations in this region (Ref. 35 approaches the intersection only to 20° in the α torsional angle). A complete active space self-consistent-field (CASSCF) calculation approaching TDDFT in accuracy requires a large active orbital space.[36] But at this stage, our

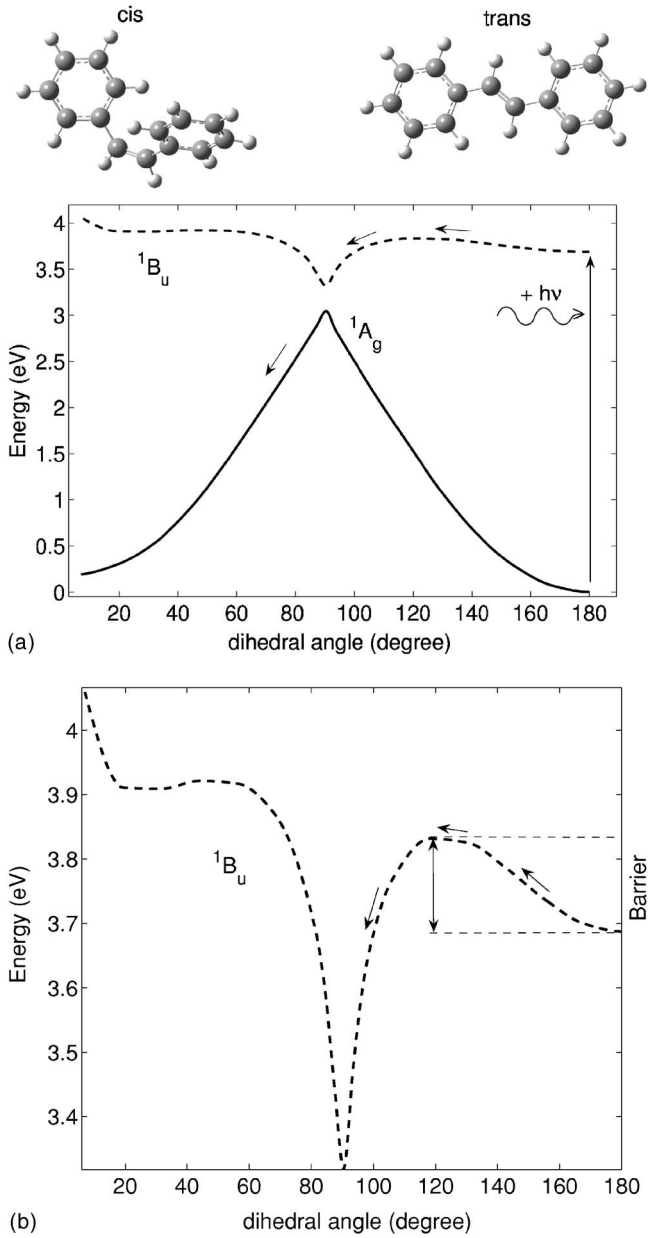

FIG. 2. (a) Potential energy surface of the ground state and the S_1 state of stilbene. (b) Zoom of the PES.

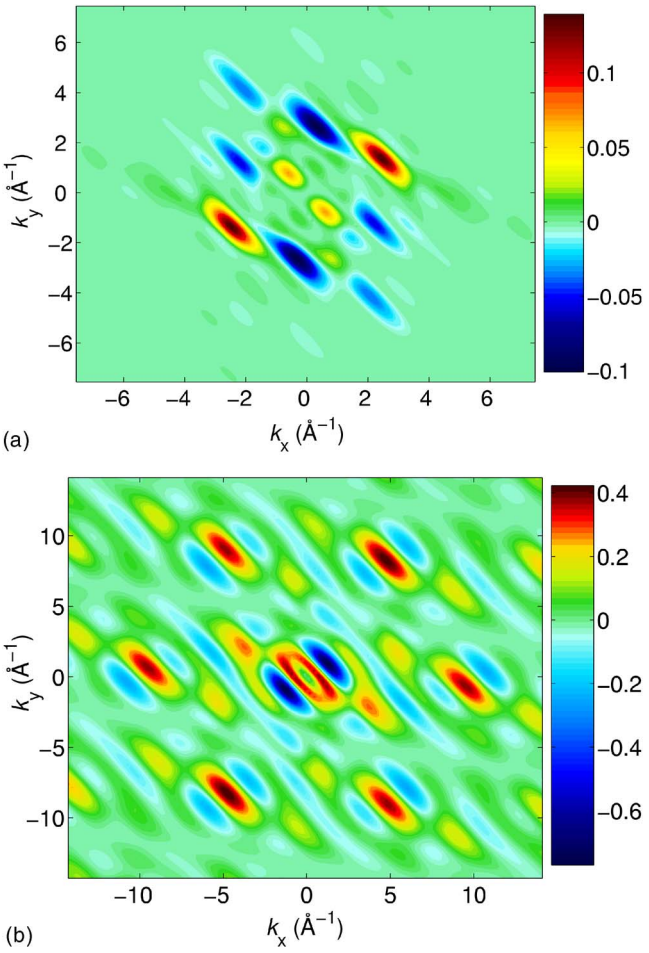

FIG. 3. (Color online) (a) Filled contour graph of the scattering intensity difference between ground state and vertically excited state in percent of $k=0$ intensity depicted on the color bar. (b) Scattering intensity difference of ground state and core excited state. For both cases we assume single-molecule scattering on *trans*-stilbene.

main reason for obtaining the reaction path is the following study of the isomerization dynamics in order to investigate the scattering signal differences as obtained from classical or quantum-mechanical calculations. Although approximate, the chosen reaction path is sufficient as a base for our further calculations where we take snapshots of the electron density along the reaction path by calculating the single-molecule scattering signal.

B. The x-ray scattering patterns

Before integration, the $|\mathcal{F}_{\mathbf{k}}\{\rho(\mathbf{r},t)\}|^2$ term in Eq. (19) corresponds to x-ray scattering at one molecule. This is naturally much more sensitive to electron density changes than the WAXS signal which is averaged for random orientations of molecules. For a better insight into the problem, we will first show the difference in the single-molecule scattering from two different electron density distributions (and later on compare to a randomly oriented molecular ensemble as been described by the Debye equation).

We start with a calculation of the signal change in the case of the smallest typical electron density change, namely, highest occupied molecular orbital (HOMO)–lowest unoccupied molecular orbital (LUMO) excitation of *trans*-stilbene. Figure 3(a) shows the difference signal from the single-molecule scattering of *trans*-stilbene in the ground electronic state and first excited Franck-Condon state. As we see, the maximum signal difference in this case is about 0.14% [given in percent of the $k=0$ intensity, that is, $\Delta I/I(k=0) \times 100$]. Stronger signal changes can be expected if we remove one electron from a strongly localized core state (on one central carbon atom) and excite it into the LUMO. Indeed the calculated absolute difference of the scattering signal amounts to 0.78% [Fig. 3(b)].

The differences in the single-molecule scattering signal that come from electron density changes caused by changes in orbital occupancies are only subtle. We can compare them with the single-molecule scattering differences due to large geometry changes. Figure 4(a) represents the difference in the signal from *trans* and *cis* isomers, and Fig. 4(b) the dif-

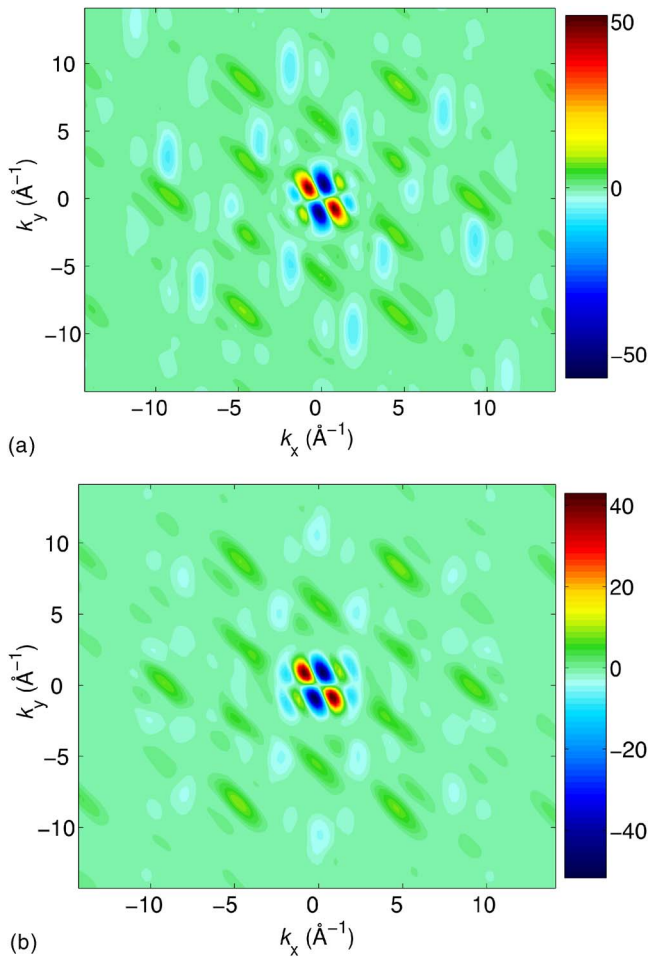

FIG. 4. (Color online) (a) Filled-contour graph of the scattering intensity difference between *trans* and 130° state in percent of $k=0$ intensity depicted on the color bar. (b) Scattering intensity difference of *trans* and *cis* states.

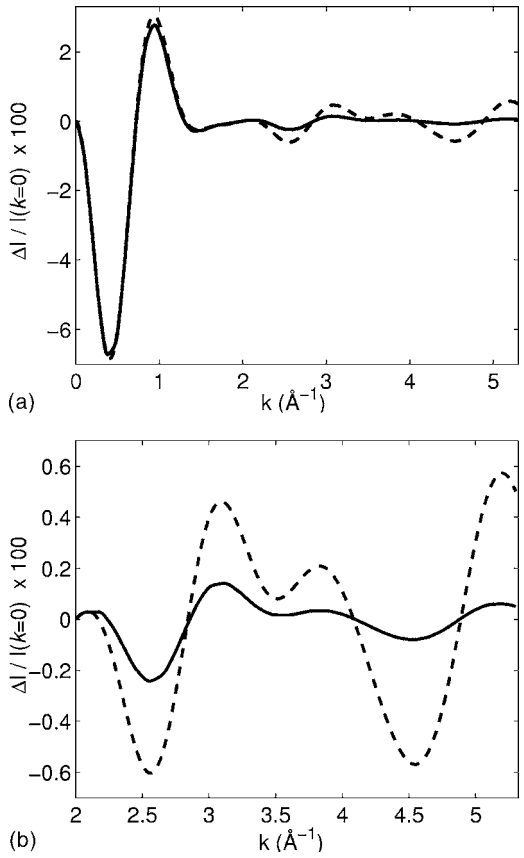

FIG. 5. (a) WAXS difference signal as given by the Debye equation (dashed line) vs signal from the DFT/B3LYP electron densities (solid line). (b) Detail of the WAXS difference signal at higher k values.

ference in the signal from *trans* and 130° dihedral angle geometry. The absolute difference [when normalized to $\Delta I/I(k=0)\times 100$ which means percent of the $k=0$ intensity] is high (around 55%), however, this is not as strongly pronounced in the WAXS patterns since the negative and positive contributions cancel each other.

WAXS scattering signals are averaged over the spherical angles of single-molecule scattering. Compared to the latter case, this averaging obviously leads to a loss of details in the scattering patterns. The following results show what kind of effects are the WAXS patterns sensitive to if coming from a detailed description of the electron density, and later showing the sensitivity of the WAXS signal to the wave-packet description of the molecular degrees of freedom.

In the following we call the difference in the WAXS intensity from two different molecular geometries at the same level of electron density assessment (Debye equation or detailed density approach) "difference intensity." As we can see from Figs. 5(a) and 5(b), respectively, the *trans* to *cis* difference intensities as given by the Debye equation and direct Fourier transformation of electron densities are in good agreement approximately up to $k=2$ Å^{-1}. From here the difference between these two approaches starts to grow with higher k. It amounts to 0.3% at $k=3.1$ Å^{-1} [when normalized to $\Delta I/I(k=0)\times 100$ or percent of the $k=0$ intensity], which in relative terms means that the Debye equation overestimates the difference signal by a factor of 3.3 at this k point. At $k=5.2$ Å^{-1} it grows to 0.5% which means a factor of 9.3 overestimation by the Debye equation. We should point out that the region of higher k values is the one where the effects of more localized changes in geometry become pronounced. The periodicity and the main features of the difference intensity remain the same.

By comparing the WAXS scattering intensities derived from the Debye equation with those derived out of the first principles, the deviations at the same geometry become pronounced at $k\simeq 0.5$ Å^{-1} and the difference grows to approximately 3% at $k=3$ Å^{-1} as the signal from the detailed density decreases faster than the Debye signal. However, since the detailed electron density brings the similar delocalization to every geometry, the WAXS signal from every geometry decreases in the same manner which causes the difference intensities from the detailed density to be approximately ten times smaller as compared to the Debye difference intensity. The differences between classical scattering description and scattering differences derived from first principles might already be envisited by using Pink-Laue type of high-resolution WAXS experiments at current synchrotrons of the third generation with about 10^8 photons per pulse and energies above 20 keV.[46]

C. Dynamics

In order to estimate the time scale of the process we have performed a classical simulation of the dynamics on the calculated PES, using the standard Verlet integration[47,48] of the equation of motion. In the case of the photoisomerization of stilbene, this can offer only an order-of-magnitude guess about the time scale, since for full consideration the nonadiabaticity of the process must be assessed. Instead of taking into account the two state system we assume a simple path from the Franck-Condon state to the *cis* ground state over the conical intersection as if it would belong to a single state. In the chosen internal coordinates described in Sec. III A the PES to a large extent changes smoothly and a small number of points are sufficient for the energy calculation. We formed the calculation in 22 points with higher density of points at the intersection, and for the further calculations we increase the number of points with a simple quadratic spline on the obtained surface. The Verlet integration on this approximate minimal energy photoisomerization path. In this way we approximate the time scale of the process to be on the order of picoseconds (about 2 ps, depending on the initial kinetic energy), with a fast relaxation from the first excited state to the ground state through the conical intersection in the time scale on the order of femtoseconds (about 200 fs). The small initial kinetic energy used is just sufficient for the molecule to cross the small barrier in the excited state.

Some attention should be payed to the choice of the active coordinates. We have simplified the problem to one internal coordinate—the reaction path. This is by definition also the coordinate with the weakest confinement for vibrational motion. Including more than one dimension brings about problems in the integration according to Eq. (19) since the number of analytical functions needed for the description of the density of the wave packet grows accordingly and the calculation becomes very time consuming. Note that the final simulated WAXS signal changes based on the Debye equation correspond to an optical excitation with circularly polarized light leading to a homogeneous distribution of photoexcited chromophors. Under this assumption the dephasing effects for orientational distribution can be ignored.

In the following we present the studies on the influence of the wave-packet description of nuclear degrees of freedom on the WAXS signal and the difference intensities. Since at this stage we are not interested in a rigorous description of the isomerization reaction path, but rather in the possible effects which the wave-packet description can have on the scattering patterns, we will employ some simplifications. The calculation of the wave-packet dynamics on our surface (as in the Verlet integration case) is performed in a standard split-operator procedure.[49] We include a small initial momentum to make the molecule move in one direction across the barrier. Figure 6 shows the first 250 femtoseconds of the photoisomerization process. The ground state wave packet is strongly confined by the ground state potential. As we could predict the WAXS signal of this well localized wave packet is practically indistinguishable from the signal as coming from the *trans* single geometry electron distribution. After vertical excitation ($t=0$) the wave packet quickly broadens

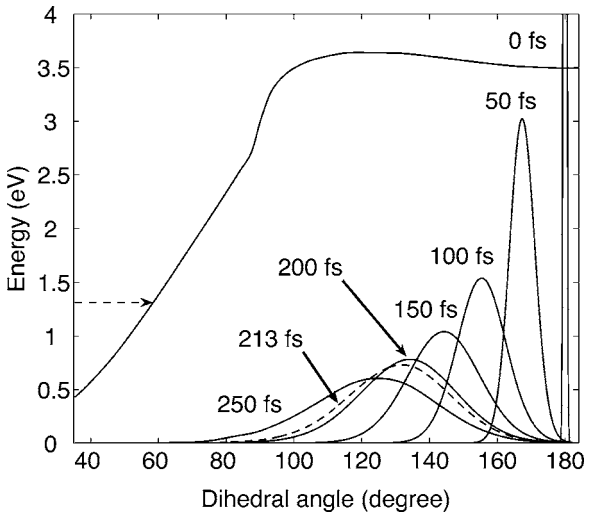

FIG. 6. Wave-packet dynamics in the first 250 fs of the photoisomerization process. The PES used in the dynamics calculation is shown for clarity. Both the PES and the wave-packet evolution are ploted vs the dihedral angle.

on the shallow S_1 surface during the isomerization process (see Fig. 6). In order to compare the classical and wave-packet approaches to the time development of scattering patterns we calculate these patterns at different time points of the isomerization process. We choose the *trans* ground state, the wave packets in the first 60 femtoseconds of the process and a later wave packet at 214 fs, the expectation value of which corresponds to a geometry with dihedral angle $\alpha = 130.6°$. The later wave packet is chosen as one which corresponds to the excited state before the transition over the conical intersection because of our choice of the simplified reaction path. The x-ray scattering from a wave packet can be treated in two different ways. We can assume times shorter than the internal vibrational redistribution decoherence time, which is expected to be about 50–100 fs. At this very short time scales the nuclear degrees of freedom are described as coherent wave packets. The second case corresponds to times when decoherence is pronounced in the system either due to vibrational redistribution or interaction, e.g. collisions, with the molecules from the environment. Here the wave packet corresponds to a probability distribution of specific geometries in an ensemble of molecules.

Let us first consider the first, coherent case. The electron density of a system can be expressed as the expectation value,

$$\rho(\mathbf{r}(t)) = \langle \chi(\mathbf{R},t) | \rho(\mathbf{r},\mathbf{R},t) | \chi(\mathbf{R},t) \rangle, \tag{22}$$

where $\chi(\mathbf{R},t)$ corresponds to the nuclear wave packet with nuclear coordinates $\mathbf{R}$. This electron density employed is an average over the nuclear wave function, as described in Eq. (22). In this way we get a delocalization in electron density due to the wave-packet description of the nuclear degrees of freedom. Figure 7 shows the difference intensities from the coherent wave packets corresponding to $t_0(0\text{ fs}) - t(10,20,30,40,50,60\text{ fs})$ and for comparison also the difference intensity coming from the ensemble wave-packet description at times $t_0(0\text{ fs}) - t(10,60\text{ fs})$. The decrease in WAXS intensity caused by the electron density delocaliza-

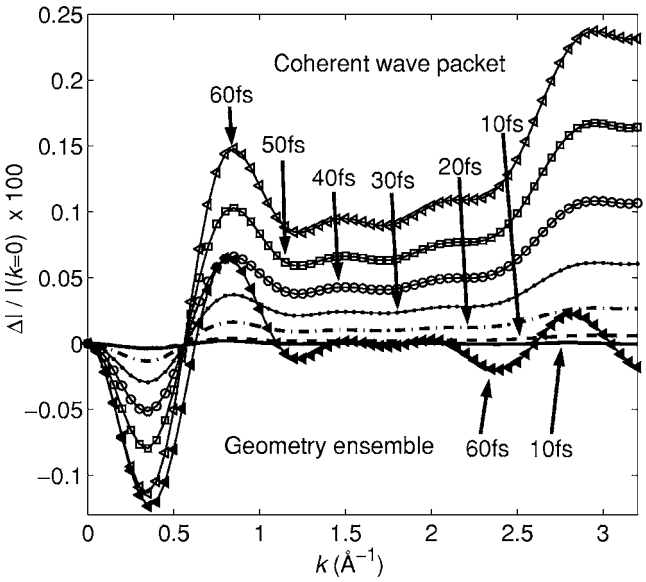

FIG. 7. WAXS difference intensity as simulated from the wave-packet dynamics at $t=0-(10,20,30,40,50,60)$ fs coherent wave packets, compared to the intensity from an ensemble with geometry probabilities corresponding to the wave packet at $t=0-(10,60)$ fs.

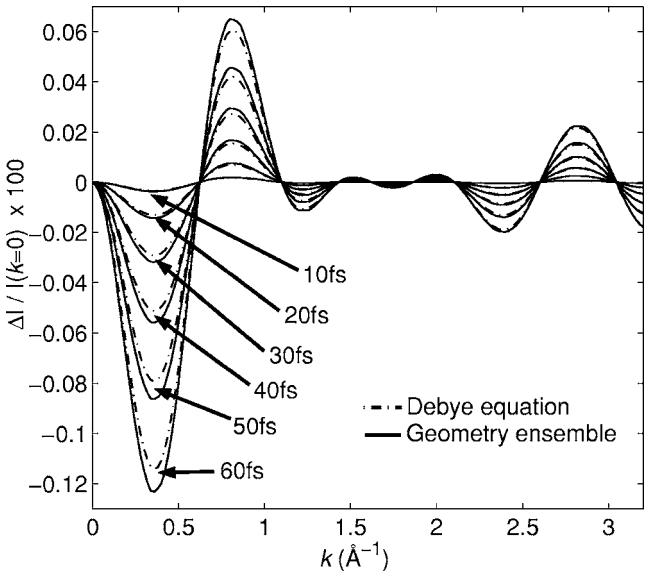

FIG. 8. WAXS difference intensity as simulated from the Debye equation (solid line) at the expectation value of the nuclear geometry at $t=0-(10,20,30,40,50,60)$ fs coherent wave packets, compared to the intensity from an ensemble with geometry probabilities corresponding to the incoherent wave packet at the same time points (dashed line).

tion in the coherent wave packet is strong. As the wave packet broadens in time on the shallow S_1 surface, the electron density delocalizes accordingly. The WAXS intensity from a broad wave packet is decreased in comparison with the WAXS intensity from a more localized wave packet at an earlier time point. The difference intensity for two different times t_0-t then grows with increasing time t, in particular, at higher k values since $t_0=0$ corresponds to the sharply localized Franck-Condon wave packet. The comparison with the corresponding difference intensities as calculated using the expectation geometry in the Debye equation and the incoherent wave packet described by the probability distribution of the nuclear geometries is made in Fig. 8. As we can see here, the signal from the geometry ensemble shows only very small changes to the Debye equation difference signal at the expectation value of the particular wave packet in the k range up to 3 $Å^{-1}$.

After the coherence of the wave packet is destroyed by molecular vibrations and collisional interactions, the wave packet corresponds to the incoherent probability distribution. For the sake of the test of the method we choose the wave packet after 213 fs (with the expectation value corresponding to 130.6°) and calculate the WAXS signal using Eq. (19) with integration over the wave-packet geometry ensemble included. Although the WAXS signal from this kind of ensemble is not equal to the signal from the expectation value geometry, the calculated difference between them is in our case very small and no characteristic effect is observable, similarly to earlier time points of the isomerization process shown in Fig. 8.

IV. CONCLUSIONS

As the experimental equipment gradually enables us to study liquid samples by WAXS measurements, it is important to reflect on the theory commonly used, in this case the Debye equation, which ignores the difference between the classical model of electron density and the more rigorous quantum-chemical approach. As we have shown, this classical approach can be used only at small k values (from 0 to approximately 2 $Å^{-1}$) which means the k range where large-scale electron density effects are observable. In the range of k values, where actual molecular geometry effects can be observed, electron delocalization becomes increasingly important and omitting quantum effects would lead to a misinterpretation of the scattering patterns. In particular, the Debye equation overestimates the sensitivity of WAXS which can be misleading when interpreting experimental data.

The time-dependent calculation of the scattering signal from the wave-packet dynamics has important implications. Assuming that *trans*-stilbene is in a low-lying vibrational state (ground state in our case) the corresponding wave packet can be considered as strongly localized. After a Franck-Condon excitation from this ground state the wave packet broadens as it follows the reaction path. The broadening of the wave packet which corresponds to a vibrational redistribution in the excited state is observable in the further broadening of the scattering patterns. Evolution of the overall wave packet in time is so observable in the scattering patterns. Both effects, the consideration of real electron density distribution and in the time-resolved case the consideration of nuclear degrees of freedom described by a wave packet, bring a considerable decrease of the intensity of the WAXS signal, in particular, at high k values. However, in the case of the wave-packet calculations the dynamic interaction of x-rays with the molecule must be considered, which will be a task for our further studies.

ACKNOWLEDGMENTS

S.T. is grateful for support by the Deutsche Forschungsgemeinschaft (TE 347/1-2,3). S.S. thanks the Fonds der Chemischen Industrie for financial support.

[1] R. Neutze, R. Wouts, S. Techert, J. Davidsson, M. Kocsis, A. Kirrander, F. Schotte, and M. Wulff, Phys. Rev. Lett. **87**, 195508 (2001).
[2] S. Techert, F. Schotte, and M. Wulff, Phys. Rev. Lett. **86**, 2030 (2001).
[3] J. Davidsson, J. Poulsen, M. Cammarata *et al.*, Phys. Rev. Lett. **94**, 245503 (2005).
[4] H. Ihee, M. Lorenc, T. K. Kim, Q. Y. Kong, M. Cammarata, J. H. Lee, S. Bratos, and M. Wulff, Science **309**, 1223 (2005).
[5] A. M. Lindenberg, Y. Acremann, D. P. Lowney, P. A. Heimann, T. K. Allison, T. Matthews, and R. W. Falcone, J. Chem. Phys. **122**, 204507 (2005).
[6] S. Techert and S. Schmatz, Z. Phys. Chem. **216**, 575 (2002).
[7] V. Srajer, T. Y. Teng, T. Ursby, C. Pradevard, Z. Ren, S. Adachi, W. Schildkamp, D. Bourgeois, M. Wulff, and K. Moffat, Science **274**, 1726 (1996).
[8] C. Bressler and M. Chergui, Chem. Rev. (Washington, D.C.) **104**, 1781 (2004).
[9] A. Rousse, C. Rischel, S. Fourmaux *et al.*, Nature (London) **410**, 65 (2001).
[10] K. Sokolowski-Tinten, C. Blome, J. Blums *et al.*, Nature (London) **422**, 287 (2003).
[11] T. Lee, Y. Jiang, C. G. Rose-Petruck, and F. Benesch, J. Chem. Phys. **122**, 084506 (2005).
[12] C. Rose-Petruck, R. Jimenez, T. Guo, A. Cavalleri, C. W. Siders, F. Raksi, J. A. Squier, B. C. Walker, K. R. Wilson, and C. P. J. Barty, Nature (London) **398**, 310 (1999).
[13] A. M. Lindenberg *et al.*, Science **308**, 392 (2005).
[14] Technical Report No. SLAC-R-593 LCLS, edited by J. Arthur, 2002, www.ssrl.stanford.edu (unpublished).
[15] Technical Report No. 3, edited by G. Materlik and T. Tschentscher, 2003 (unpublished); see www-habylab.desy.de
[16] D. H. Bilderback, P. Elleaume, and E. Weckert, J. Phys. B **38**, 773 (2005).
[17] H. Köppel, W. Domcke, and L. S. Cederbaum, Adv. Chem. Phys. **57**, 59 (1984).
[18] J. L. Krause, R. Whitnell, K. R. Wilson, and Y. J. Yan, J. Chem. Phys. **99**, 6562 (1993).
[19] B. Kohler, V. V. Yakovlev, J. Che, J. L. Krause, M. Messina, and K. R. Wilson, Phys. Rev. Lett. **74**, 3360 (1995).
[20] P. Hohenberg and W. Kohn, Phys. Rev. **136**, 864 (1964).
[21] D. Feil, Isr. J. Chem. **16**, 103 (1977).
[22] D. Feil, J. Mol. Struct.: THEOCHEM **255**, 221 (1992).
[23] V. G. Tsirelson and R. P. Ozerov, J. Mol. Struct.: THEOCHEM **87**, 335 (1992).
[24] P. Coppens, *X-ray Charge Densities and Chemical Bonding* (Oxford University Press, Oxford, 1997).
[25] S. F. Boys, Proc. R. Soc. London, Ser. A **258**, 402 (1960).
[26] J. A. Syage, P. M. Felker, and A. H. Zewail, J. Chem. Phys. **81**, 4685 (1984).
[27] K. Ishii, S. Takeuchi, and T. Tahara, Chem. Phys. Lett. **398**, 400 (2004).
[28] J. Schroeder and J. Troe, in *Activated Barrier Crossing*, edited by G. R. Fleming and P. Haenggi (World Scientific, Singapore, 1993).
[29] J. A. Syage, W. Lambert, P. M. Felker, A. H. Zewail, and R. Hochstrasser, Chem. Phys. Lett. **88**, 266 (1982).
[30] J. Troe and K.-M. Weitzel, J. Chem. Phys. **88**, 7030 (1988).
[31] M. W. Balk and G. R. Fleming, J. Phys. Chem. **90**, 3975 (1986).
[32] J. Schroeder, D. Schwarzer, J. Troe, and F. Voss, J. Chem. Phys. **93**, 2393 (1990).
[33] R. Mohrschladt, J. Schroeder, J. Troe, and P. Vöhringer, J. Chem. Phys. **101**, 7566 (1994).
[34] C. Dietl, E. Papastathopoulos, P. Niklaus, R. Improta, F. Santoro, and G. Gerber, Chem. Phys. **310**, 201 (2005).
[35] R. Improta and F. Santoro, J. Phys. Chem. A **109**, 10058 (2005).
[36] L. Gagliardi, G. Orlandi, V. Molina, P.-Å. Malqvist, and B. Roos, J. Phys. Chem. A **106**, 7355 (2002).
[37] B. E. Warren, *X-Ray Diffraction* (Addison-Wesley, Reading, MA, 1969).
[38] M. J. Frisch, G. W. Trucks, H. B. Schlegel *et al.*, GAUSSIAN 03, Gaussian, Inc., Wallingford, CT, 2004.
[39] A. Becke, J. Chem. Phys. **104**, 1040 (1996).
[40] C. Lee, W. Yang, and R. Parr, Phys. Rev. B **37**, 785 (1988).
[41] A. D. Becke, J. Chem. Phys. **98**, 5648 (1993).
[42] J. D. Pedrew, Phys. Rev. B **33**, 8822 (1986).
[43] K. B. Wiberg, A. E. de Oliveira, and G. Trucks, J. Phys. Chem. A **106**, 4192 (2002).
[44] P. M. Felker and A. H. Zewail, J. Phys. Chem. A **89**, 5402 (1985).
[45] D. M. Leitner, B. Levine, J. Quenneville, T. J. Martínez, and P. G. Wolynes, J. Phys. Chem. A **107**, 10706 (2003).
[46] A. Debnarova, M. Goulakov, N. Petrov, M. Camaratta, M. Wulff, S. Schmatz, and S. Techert (in preparation).
[47] L. Verlet, Phys. Rev. **159**, 98 (1967).
[48] L. Verlet, Phys. Rev. **165**, 201 (1968).
[49] M. D. Feit, J. A. Fleck, Jr., and A. Steiger, J. Comput. Phys. **47**, 412 (1982).